THE INCISION PATTERN OF CONSEQUENT STREAM INTO INCREASING UPLIFT

Dr. N.L. Dongre, IPS, Ph.D., DLitt**

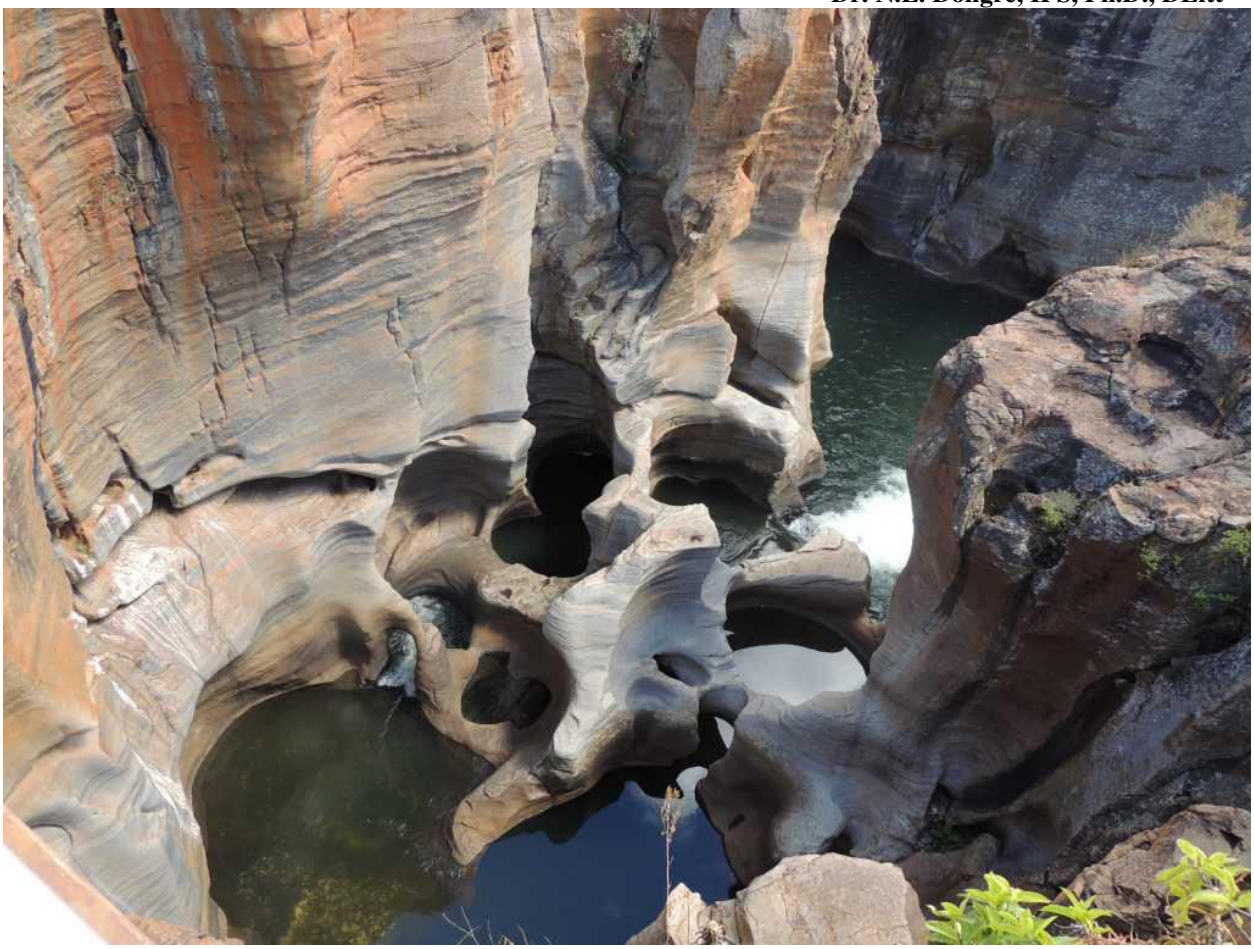

The incision pattern indicates that initial channel incision is latest near the uplift toe, bu migrates upstream with time as the progression of channel reflect from potehole nearby Dhupgarh mountain of Pachmarhi.

[1] No sooner as uplift begins to increase above base level, than it subjects to erosion. A numerical model of simultaneous uplift growth and river erosion captures the early stages of channel formation and delineates the evolution of longitudinal channel profiles. This numerical exploration suggests that the patterns of channel incision into increaing uplifts can be used to guide kinematic interpretations of uplift growth. Four types of uplift limb growth are modeled: limb lengthening through (1) the uplift crest or (2) the uplift toe, (3) limb rotation, and (4) curved uplift limbs due to trishear uplifting. Initially, the pattern of channel incision is sensitive to the kinematics of surface deformation. Subsequently, more mature streams evolve toward identical incision patterns with deepest incision near the midpoint of the longitudinal channel profile. It is compared that these model predictions to the Pachmarhi Mountain in India, where high-resolution topographic data reveal the multitude of channels incised into the flanks of these uplifts. As the opposing limbs of these uplifts have followed distinct deformation pathways, the early sensitivity of channel incision to deformation pathway can be examined.

**Dr. N.L. Dongre
C-14 Jaypee Nagar Rewa 486450
Email: - nl.dongre@jalindia.co.in dongrenl@gmail.com
Mobile No. 7869918077, 09425152076

Furthermore, the lateral propagation of the uplift through time allows for an approximate space-for-time substitution, such that the evolution of these incision patterns can be examined from early through more mature stagesThis analysis indicates that the west limb of the Pachmarhi has increased by limb lengthening through the toe and the east limb has increased primarily by lengthening through the crest.

Keyword: uplift, consquent stream, kinematic deformation, incision, Pachmarhi downstream, . Mahadeva, spatial pattern.

Introduction

[2] Uplifted unconformities preserved either in growth strata or as fluvial terraces are commonly exploited as incremental strain markers to infer the kinematics of uplift growth *[Daeron et al.,* 2007; *Hubert-Ferrari et al.,* 2007; *Lave and Avouac,* 2000; *Wilson et al.,* 2009], but such unconformities are not ubiquitously preserved, nor do they necessarily indicate a unique deformation pathway. Here it is considered that the incision pattern of consequent streams, those that form due to uplift growth, as another indicator of uplift growth history. Although the insights gained from the patterns of channel incision suffer from the same limitations of limited preservation and ambiguity, such insights are based on a different set of assumptions. For example, the assumption of nearly instantaneous abandonment of a wide channel cut surface to form a terrace is not required. Similarly, the assumption of isochrony for stratigraphic horizons used to delineate growth strata is unnecessary. River incision profiles can, therefore, provide an additional piece of questions of uplift kinematics even in the presence of steady hydrologic and tectonic conditions.

2. Simple Models of Uplift Growth

[3] Imagine a tilted geomorphic surface that is 1 km long from crest to toe and has a constant dip of 10°. Some combination of three end-member kinematic histories (Figure 1) could produce such a structure: (1) while always maintaining a constant limb dip, the surface could have been laterally advected through a synclinal hinge at the toe of the uplift; (2) the uplift limb could have remained 1 km long for its entire history and rotated to achieve a dip of 10°, or (3) the surface could have been laterally advected through an anticlinal hinge at the uplift crest while maintaining constant dip *[Ahmadi et al.,* 2006; *Wilson et al.,* 2009]. These geometric growth patterns can be associated with specific fault geometries that could lead to their formation (Figures 1a and 1b), namely, a fault bend uplift *[Suppe,* 1983; *Suppe et al.,* 1997] and a listric thrust fault *[Amos et al.,* 2007; *Erslev,* 1986]. Given that other mechanisms such as detachment uplifting *[Scharer et al.,* 2004] could produce similar surface deformation patterns, it is considered that pure lengthening and rotation of a uplift limb, rather than explicitly including an underlying fault geometry. Real deformation processes likely involve some combination of rotation and lengthening, and they rarely result in perfectly planar surfaces. For this reason, it is also considered that a curved limb geometry (Figure 1c) that may form in trishear-style uplifting [Erslev, 1991; Hardy and Poblet, 2005; Zehnder and Allmendinger, 2000].

[4] It is used a numerical model to investigate how these deformation pathways can affect the pattern of incision by stream channels that form on a deforming uplift limb. In all cases, it is assumed that the uplift is fully emergent, such that its limbs rise above an unchanging local base level and are not being mantled with growth strata. This simplification of real, and possibly complex, fluctuations in base level is likely appropriate to the modeled spatial and temporal scale because (1) nascent channels on newly emergent structures may form with little connection to an established regional fluvial network and (2) channel head migration is not initially driven by headward erosion of existing channels.

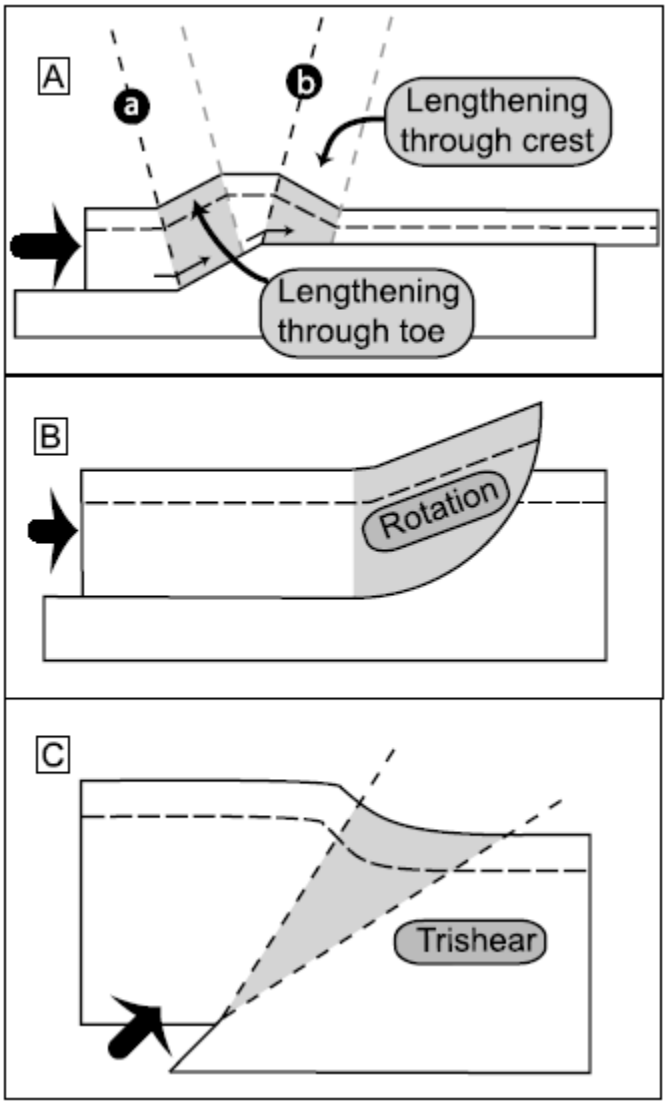

Figure 1. Schematic representations of end-member uplift growth models. (a) Limb lengthening through the toe and crest explained here as the result of deformation above a fault bend uplift. During early growth, hanging wall material moves through uplift axes *a* and *b* which are stationary with respect to the footwall. (b) Limb rotation explained as deformation above a listric thrust. (c) Formation of a curved limb in the forelimb of a trishear uplift.

3. Stream Power and Channel Erosion

[5] Stream incision into a deforming surface can be modeled according to a stream power formulation *[Howard and Kerby,* 1983] modified from the work of *Oskin and Burbank* [2007]. Erosion rate (E) is calculated as

$$E = KX^{p\theta n}S^{n}, \quad (1)$$

where K is a constant (Table 1). The upstream drainage area is used as a proxy for stream discharge and is defined as X^{p} where X is the downstream distance from the drainage divide.

In applying this model to nearly straight channels formed on the flanks of uplifts, it is assumed that downstream distance is equivalent to the perpendicular distance from the divide. The value of p describes the rate of downstream drainage area accumulation which may range between 1 for "pipe-like" drainages and 2 for "box-like" drainages *[Oskin and Burbank,* 2007]. It is set p to 1.1 to represent the

nearly pipe-like drainages that often form parallel to one another on uplifts for which limb dips are >5°. The channel slope is *S,* and the exponents 9 and *n* describe the potentially nonlinear increase of erosion rate with respect to drainage area and slope. The exponents are assumed to be 0.5 and 1 in this simple model. Although this formulation is a simplistic description of the myriad processes that can cause bedrock channel erosion *[Whipple et al.,* 2000], predictions of this model regarding patterns of channel incision are not heavily dependent on the details of the erosion rule. In general, any erosion rule that describes erosion rate as an increasing function of slope and drainage area or discharge would yield broadly similar predictions.

4. Deformation Modeling

[6] Each simulation tracks the position of two markers within the 2-D model. One marker traces the preerosion surface, and a second traces the profile of the incising channel. Initially, these markers are colocated in a straight horizontal line representing an initially unincised and undeformed surface. To model limb lengthening through the toe, the deformation velocity field $\mathbf{v}(x, y)$ contains a kink at $x = a_1$ representing the toe of the uplift:

$$\mathbf{v} = D[\cos(\theta)\hat{\mathbf{x}} + \sin(\theta)\hat{\mathbf{y}}] \text{ for } x \leq a_1 \tag{2a}$$

$$\mathbf{v} = D\hat{\mathbf{x}} \text{ for } x > a_1. \tag{2b}$$

Table.1 Summary of model Parameters

Model[a]	Geometric and Model Characteristics	Trishear Uplift Characteristics
1,2	Slope of lengthening limbs (10°)	Trishear fault dip (45°)
3	Final slope of rotating limb (10°)	Trishear apical angle (40°)
1,2	Rate of limb lengthening (3 mm/yr)	Rate of slip and tip propagation (0.5 mm/yr)
1,2,3,4	Modeled time (5 x 10^5 yr)	Initial depth of trishear fault tip (650 m)
1,2,3,4	Stream power constant *K* (3 x 10^{-5})	Type of trishear deformation field (Linear)

[a]Model numbers are 1, lengthen through toe; 2, lengthen through crest; 3, rotating limb; 4, trishear.

The rate of limb lengthening is *D,* and limb dip is θ. The vectors $\hat{\mathbf{x}}$ and $\hat{\mathbf{y}}$ are unit vectors in the horizontal and vertical directions, respectively (Figure 2a).

[7] Limb lengthening through the crest is described similarly:

$$\mathbf{v} = -\boldsymbol{D}\hat{\mathbf{x}} \text{ for } x \leq a_2 \tag{3a}$$

$$\mathbf{v} = -D[cos(\theta)\hat{\mathbf{x}} + \sin(\theta)\hat{\mathbf{y}}] \text{ for } x > a_2 \tag{3b}$$

Here a_2 represents the position of the uplift crest (Figure 2b). Both of the equation sets used to describe limb lengthening dictate the surfaces experience an abrupt change in direction, but not magnitude, of displacement through the kink.

[8] The velocity of a rotating uplift limb (Figure 2c) is the same as that of any rigid body rotation. The tangentially directed velocity *v* of points at a given distance *r* from the center of a body rotating with a given angular velocity θ can be simply described by

$$v = \dot{\theta}_r.$$

Recasting this description of rotation in Cartesian coordinates allows rotation of limb with length *L* to be described by

$$\mathbf{v} = \theta[y\hat{\mathbf{x}} + (\dot{L} - x)\hat{\mathbf{y}}] \text{ for } x \leq L \tag{4a}$$

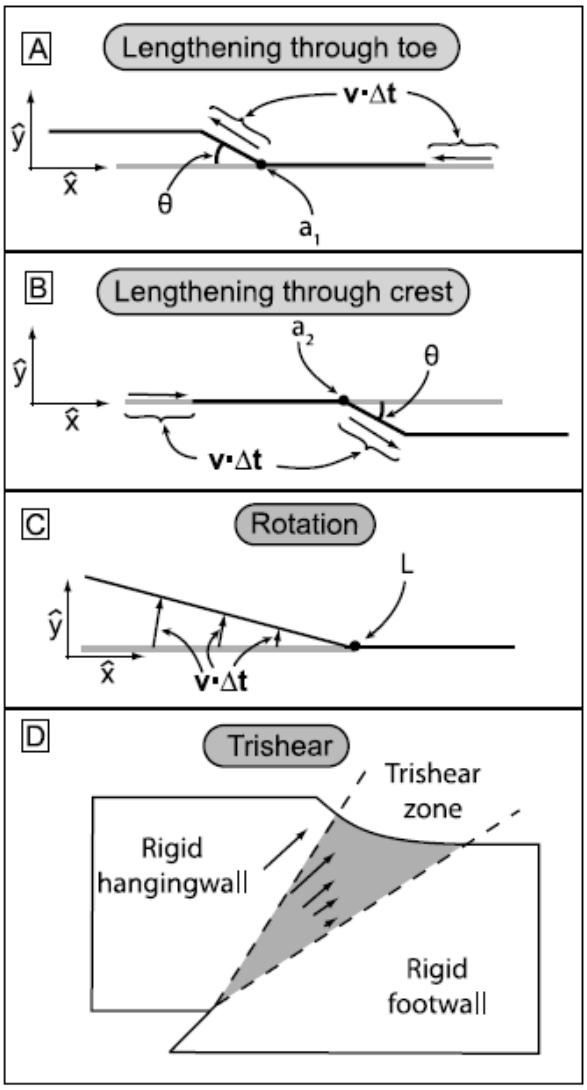

Figure 2. Setup of each of the four kinematic models of uplift limb deformation. Displacements from the initial condition (gray lines) to the deformed state (black lines) after a time Δt are shown with vector arrows. The horizontal and vertical unit vectors $\hat{\mathbf{x}}$ and $\hat{\mathbf{y}}$ are also depicted extending from the origin.

$$\mathbf{v} = 0 \text{ for } x > L. \tag{4b}$$

This description of pure limb rotation approximates the deformation pattern above a listric thrust, but does not capture the axial surface migration that occurs in such structures *[Amos et al.,* 2007].

[9] The trishear deformation field is considerably more complicated and is subdivided into the rigid hanging wall, the zone of active trishear, and the rigid footwall. Within the zone of active trishear, particle velocities are greatest at the upper boundary with the hanging wall and decrease linearly toward the lower boundary with the footwall (Figure 2d). The mathematicaldescriptions of these velocity fields are published elsewhere *[Hardy and Poblet,* 2005; *Zehnder and Allmendinger,* 2000; *Allmendinger,* 1998]. Trishear model parameters and parameters for the planar limb models are included in Table 1. It is solved for stream channel and terrace surface position through time using an explicit first-order finite difference scheme (Appendix A).

4.1. Predictions of Combined Uplift and Erosion Models

[10] Longitudinal river profiles are often used as indicators of deformation *[Kirby and Whipple,* 2001; *Stock et al.,* 2004; *Wobus et al.,* 2006]. Here, the difference in elevation between the channel and the surface into which it is incised, an incision profile, is used instead. When simultaneous erosion and deformation are modeled, a characteristic incision profile emerges depending on the deformation pathway. If the surface is deformed via lengthening such that new material is added to the limb through the uplift toe, the channel is initially most deeply incised near its midpoint (Figures 3a, 4a, and 5a). The downstream channel reaches have both a greater upstream catchment area and a steep initial slope in the newly incorporated lowest part of the limb that together lead to the fastest instantaneous incision rates, but the lower reaches have not been elevated above local base level for as much time as upstream reaches *[Ahmadi et al.,* 2006]. This mode of channel evolution is mathematically identical to the progressive exposure of a tilted, but static, surface as a less resistant cover is progressively stripped away such that base level is continuously lowered *[Oskin and Burbank,* 2007].

[11] In contrast, a channel that forms on a planar, but progressively rotating, surface is most deeply incised toward its lower end where both drainage area and stream power are greatest (Figures 3c, 4c, and 5c). Because erosion rate is calculated as an increasing function of slope and drainage area (equation (1)), the predicted incision pattern into a uplift that is formed by advection of a previously horizontal surface into the uplift limb through the crest is similar to that predicted for a rotating limb (Figures 3b, 4b, and 5b). Limb lengthening through the uplift crest increases the drainage area contributing to channel erosion.

[12] If only the longitudinal river profiles are considered (Figure 3e), important differences among the uplift growth scenarios remain. Limb rotation and lengthening through the crest produce river profiles that are more concave near the toe of the uplift than the profile produced by limb lengthening through the toe. This contrast suggests that even in the absence of a preerosion surface, some information regarding uplift growth history may be encoded in river profiles.

[13] In the case of a curved uplift limb (Figures 3d, 4d, and 5d), the concave-up shape of the surface dictates that the surface slope is much greater near the uplift crest than near the toe. As a result, incision is narrowly focused closer to the uplift crest than in the previous three models.

4.2. Evolution of Incision Profiles Through Time

[14] Incision profiles represent the cumulative effect of channel erosion. As a consequence, the channel reach experiencing the highest instantaneous erosion rates may not be the most deeply incised reach if some other reach has experienced moderate erosion rates for a longer time. This concept is illustrated in the time evolution of channels on a uplift limb that lengthens through the uplift hinge at its toe (Figure 5a). Although the predicted instantaneous incision rate will always be fastest at the toe (because it has the greatest upstream catchment area), the point of deepest incision is located well upstream of the channel toe, because the hillslope just upstream of the toe has only recently begun to incise. The exact location of deepest incision varies slightly through time depending on the sensitivity of erosion rate to the increasing length of the channel as parameterized by the values of p and 9 (equation (1)). Even though the shape of normalized incision profiles (Figure 5a) remains similar throughout model development, the channel does not reach a steady state in which incision and uplift are balanced.

[15] Deformation either by lengthening through the crest or by rotation results in channels that are initially most deeply incised near the toe of the uplift (Figures 5b and 5c). Continued deformation does not expose any new increment of the deformed surface at the uplift toe to erosion. Furthermore, the modest structural relief near the toe with respect to a fixed base level limits the depth of incision that is possible on the lower part of the uplift limb. Thus, the point of deepest incision migrates upstream once the downstream reaches have incised down to their base level of erosion.

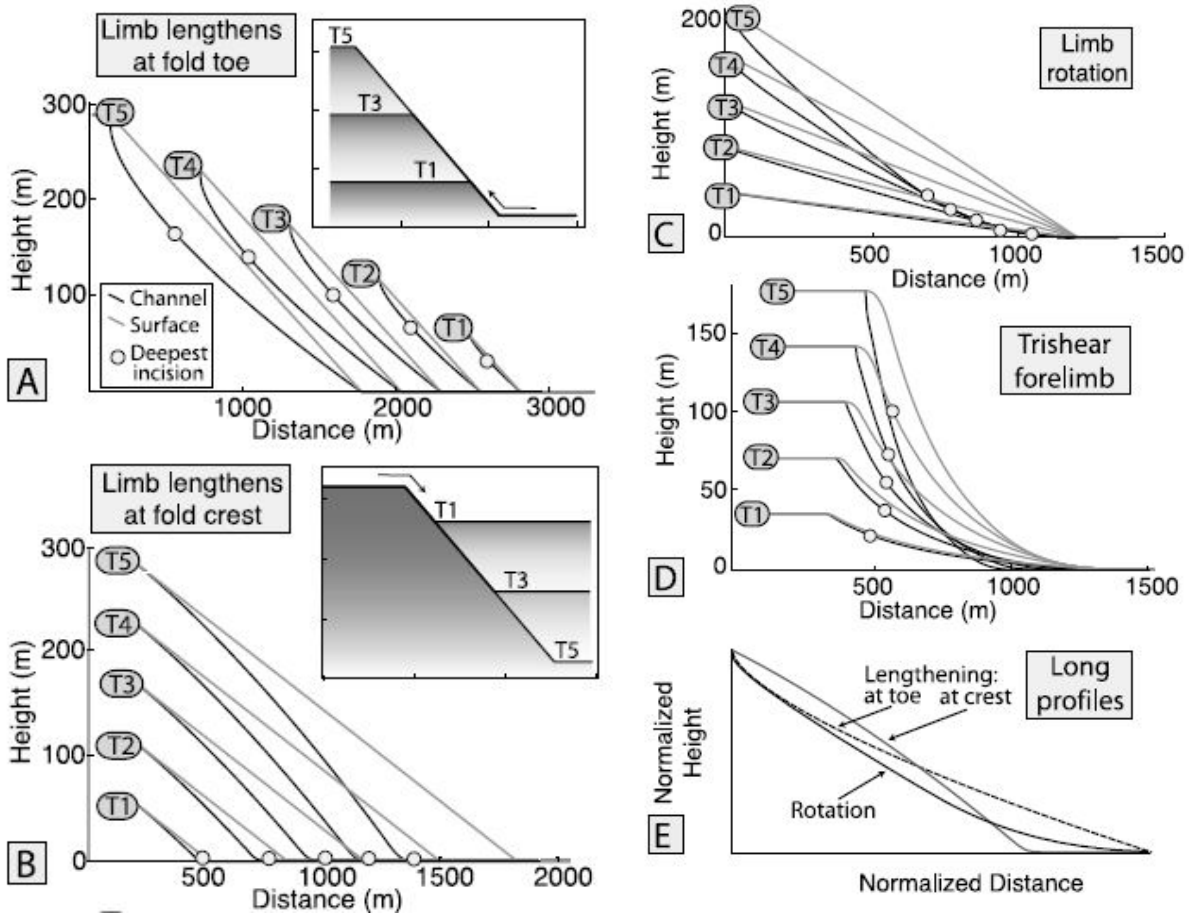

Figure 3. (A-d) Outcome of numerical model with simultaneous surface (black lines) deformation and channel (gray lines) incision from early (T1) to later (T5) stages of development. Open circles show points of deepest incision. (e) Longitudinal profiles developed at T5 for all the three models with planar uplift limbs. Though successive surface profiles overlap in the limb lengthening scenarios (Figures 3a and 3b insets), they are separated in this illustration for visual clarity.

[16] In our realization of the trishear model, the fault tip approaches the surface and, therefore, leads to a progressively narrower zone of deformation that is focused near the midpoint of the uplift limb (Figure 3d). Channel reaches near the toe of the uplift never become deeply incised because both the surface slope is gentle relative to upstream reaches and relief is low. Because a multitude of uplifting patterns (including convex uplift limbs) could be generated with different trishear model parameters, this result will not apply to every trishear uplift.

[17] In general, the modeled channels do not reach a steady state in which incision rates ubiquitously balance vertical uplift rates. In the case of limb rotation, for example, the portion of the channel nearest the toe of the uplift does approach such a balance, but the upstream reaches do not (Figure 6). The combination of relatively low uplift rates near the hinge of the rotating limb and large accumulation area allow the channel to incise at pace with uplift in its downstream reaches.

[18] The differences among incision profiles produced in this model (Figure 5) indicate that under the right conditions, stream incision patterns may be used to constrain uplift kinematics. In order for this method to be applied, it is assumed that instantaneous erosion rates are a simple increasing function of slope and drainage area. Also, remnants of the pre erosion surface must allow for its reconstruction across incised drainages. Natural examples of uplifts

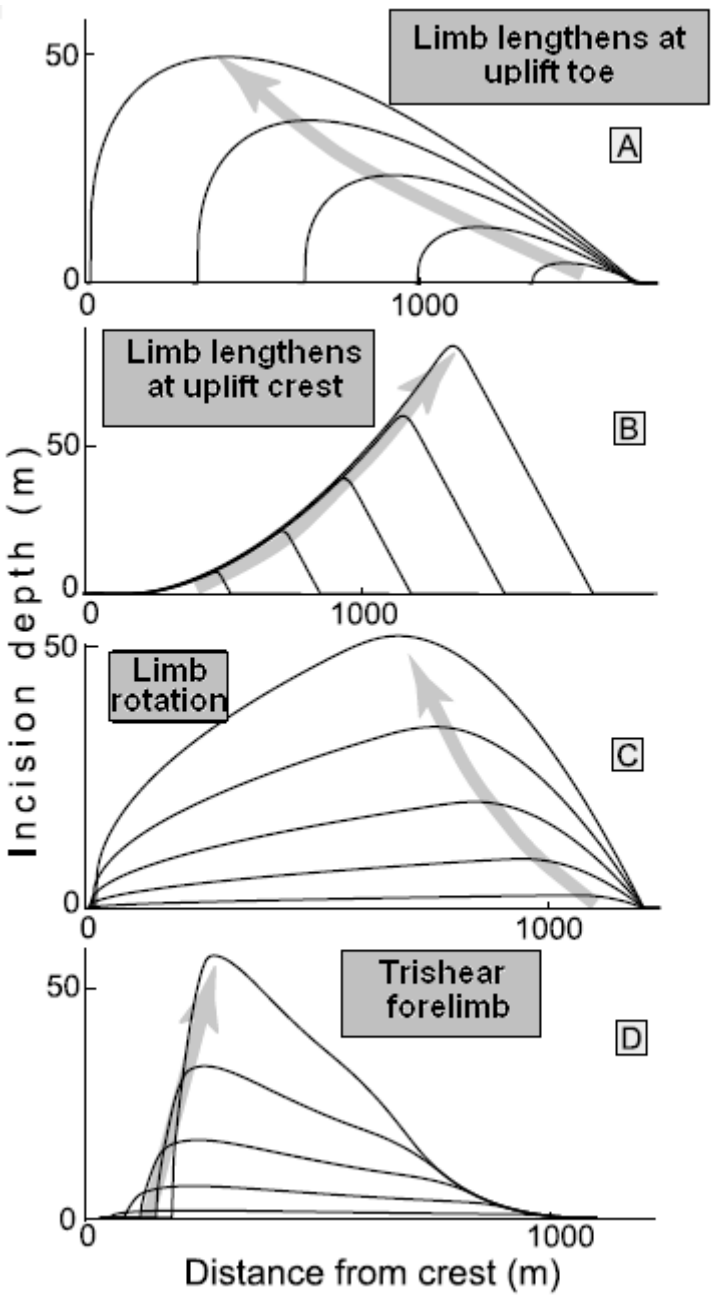

Figure 4. Depth of incision calculated as the variation between the channel elevation and pre-erosion surface at all the five stages of development shown in Figure 3.

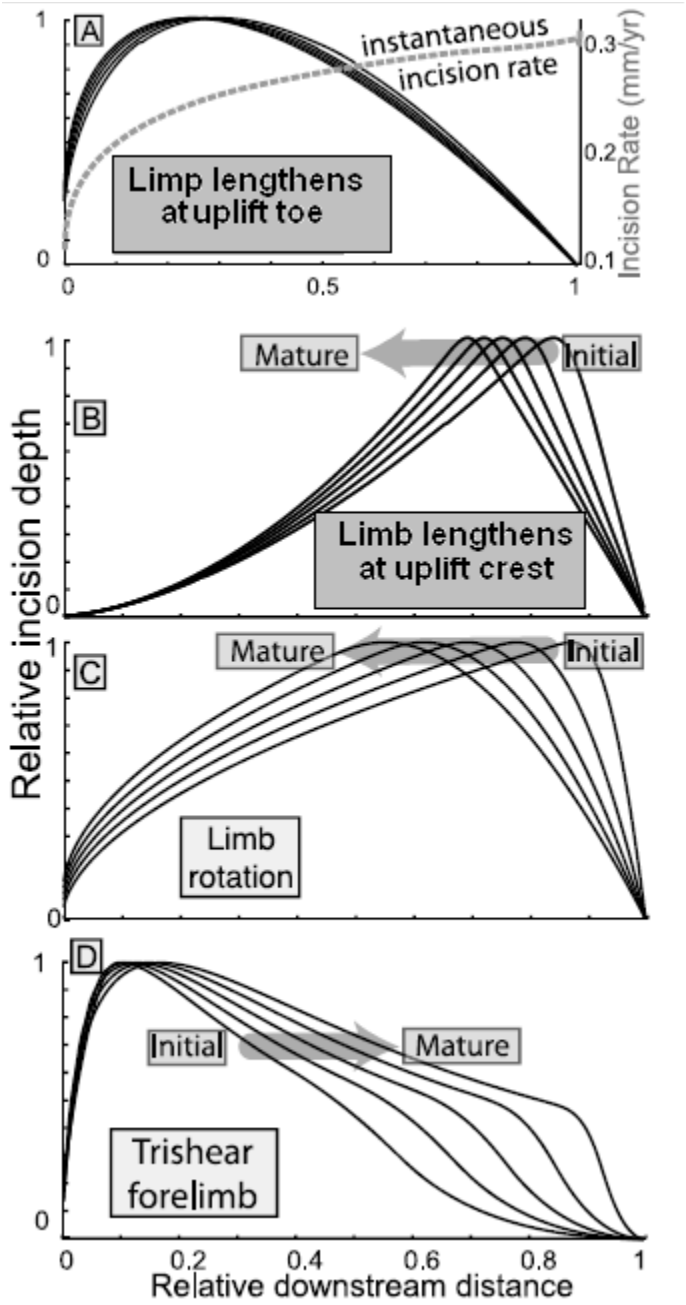

Figure 5. Modeled incision profiles plotted in terms of relative incision depth (incision depth/maximum incision depth at a given time) and relative downstream distance (distance from crest/limb length). Gray curve in Figure 5a represents instantaneous incision rate along the channel at the end of the model run.

retain a well-defined preerosion surface include the Dhupgarh,Mahadeva,Chauragarh,Belkandhar and Patalkot of Pachmarhi , Wheeler Mountain in California *[Burbank et al.,* 1996; *Keller et al.,* 1999; *Mueller and Suppe,* 1997], and the Kyrgyz and Gory Baybeiche Ranges in central Asia's Tien Shan *[Bullen,* 1999; *Oskin and Burbank,* 2007]. Each of these sites could provide a natural laboratory for testing the predictions ofour incision profile model; it is focused on one of the Mahadeva Mountain.

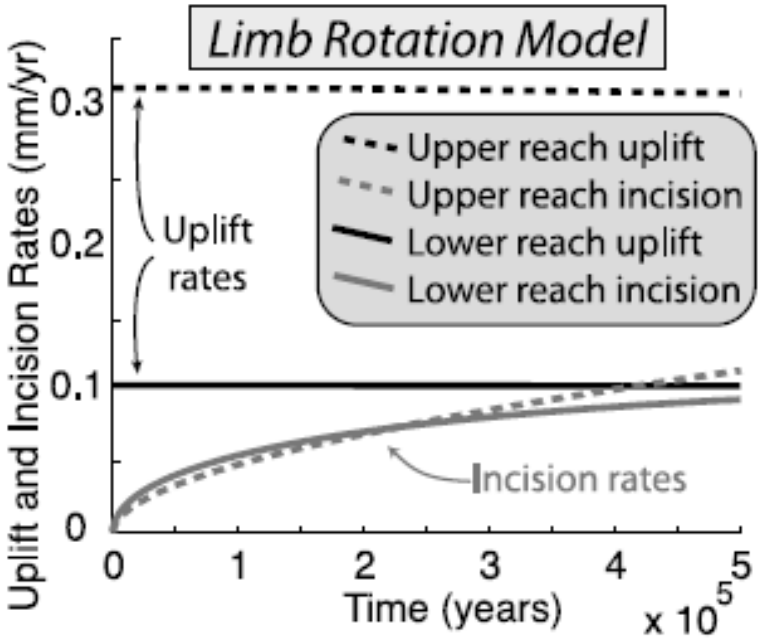

Figure 6. The approach to a steady state in the limb rotation simulation. In the lower half of the channel (solid lines), the average incision rate (gray solid line) has nearly reached the average uplift rate (black solid line). In the upper half of the channel (dotted lines), the average incision rate (gray dotted line) remains far below the average uplift rate (black dotted line).

5. Pachmarhi Mountains

[19] Pachmarhi Mountains (Dhupgarh,Mahadeva,Chauragarh and Patalkot) in India on is a southward plunging anticline formed over a blind, north dipping thrust fault. The chief features of the centre of the highland to be described is the great Mahadeva range.This mountain sloping gently northwards,but cut off to the south by a stupendous line of cliffs. The range reaches its greatest height south of Pachmarhi (22˚ 27′:78˚22′) Dhupgarh (22 27 :78 22),Mahadeo (22˚ 24′:78˚ 26′), and chauragarh (22˚ 25′:78˚ 26′), tower above the surrounding plateau, forming landmarks, All the rivers of the region originate from the trap covered high rising ranges. There is antecedent drainage system which desipher the consequent drainage after high rising of the highranges.The chief features of the drainage system is the way in which many of the rivers have cut deep channels through the highest hills.

[20] All the rivers of Pachmarhi originate in the Trap Plateaus to the south-east and south-west, though some, notably the Denwa, the Sonbhadra and the Tawa have important subsidiary source in the Mahadeva hills. All the rivers flow north through deep precipitous gorges. The chief features of the drainage system is the way in which the rivers have cut deep channels through the highest hills; The Tawa, the Denwa and Sonbhadra where they cut through the Mahadeva range. The drainage is not the result of the present topography of the country, but is due to some earlier configuration, which has now been lost owing to denudation. The present valley has faulted edges, streams, which were the ancestors of they present rivers soon became established on these uplands, and naturally flowed toward to low-lying rift valley. On the commonly preserved inter fluves, the presence of numerous 10m high tors suggest uniform lowering of the surface by slow erosion (-0.01mm/yr) over the past 1 My. The geometry of land scape is therefore, well represented by the undissected surface.

[21] In the course of denudation these streams have cut their way through the tough basalt upland. This process was naturally most rapid in the vicinity of the scrap, where erosion was greatest. Once the trap hills were reached the speed with which the valleys were carved out was greatly increase (Fig:7). The ultimate result of this denudation was to form deep gorges in the originally up rise country.

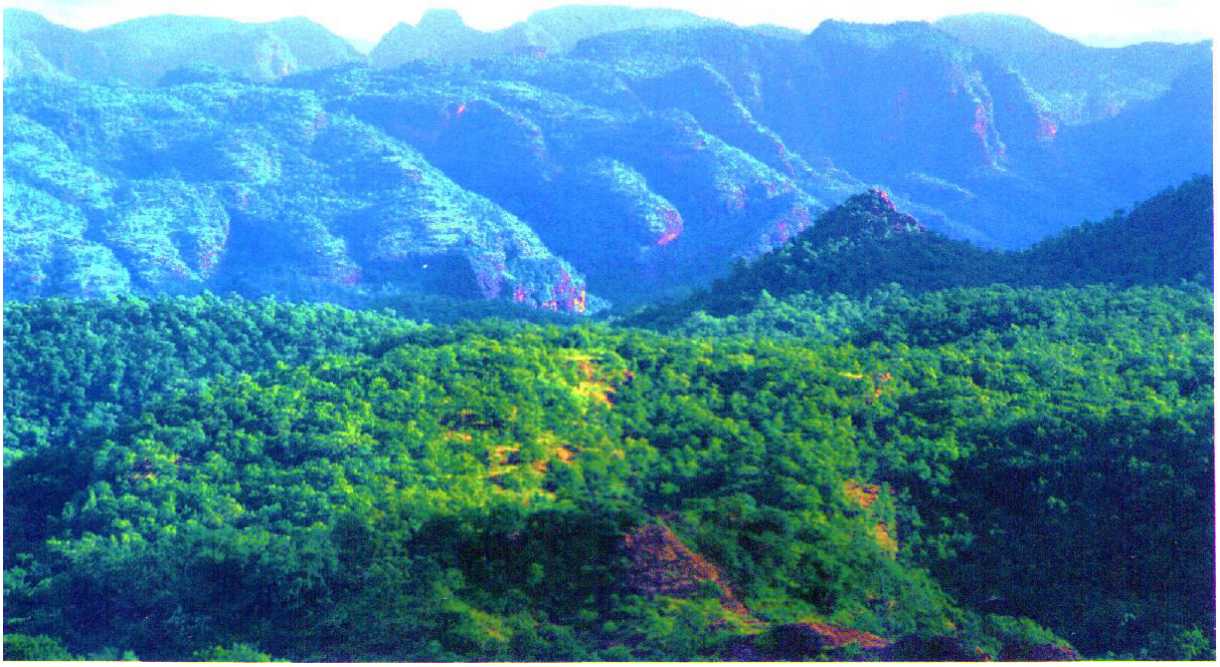

Figure 7. (a) Oblique view of Mahadeva Mountain are exposed in numoures canyons that have incised through basalt deposits into the underline bedrock. The traces of original uplift still remain inspite of river incision and they are sufficiently well preserved to be interpreted with safety.It is thought that is an ancient anticlinorium

[22] As the result of this process continued over an immense period, the diversion of many of the stream which cut through the Mahadevas to an east-west direction on the north side of those hills is a recent phenomenon. The Sonbhadra seems to have once flowed north but now debonches in to the Denwa valley. It seems to have been deflected to the west by a gradual rise of the land on the south of the Narbada plain. This movement has taken place in recent or tertiary times. The Gondwana rocks of Mahadeva-Pachmarhi have also been greatly eroded. This is naturally most marked in the gorges. The most astonishing instances occur in the Mahadeva hills. Among many wonderful instances the canyon cut right through the Mahadeva range by the Sonbhadra River is the best case. This glen is 700 mtrs deep and is a kilometer across in places. It's both sides are gigantic cliffs.

[23] The position of deepest incision along 42 minor channels on the east limb does not vary systematically along the length of the uplift and is localized near the midpoint of the uplift limb on average (Figure 9). The study area on the eastern limb encompasses north plunging uplift tips. The drainages etched into the most southerly uplift tip have headwaters that extend well above the crest of the uplift and onto the larger structure of Pachmarhi mountain (Figure 8).

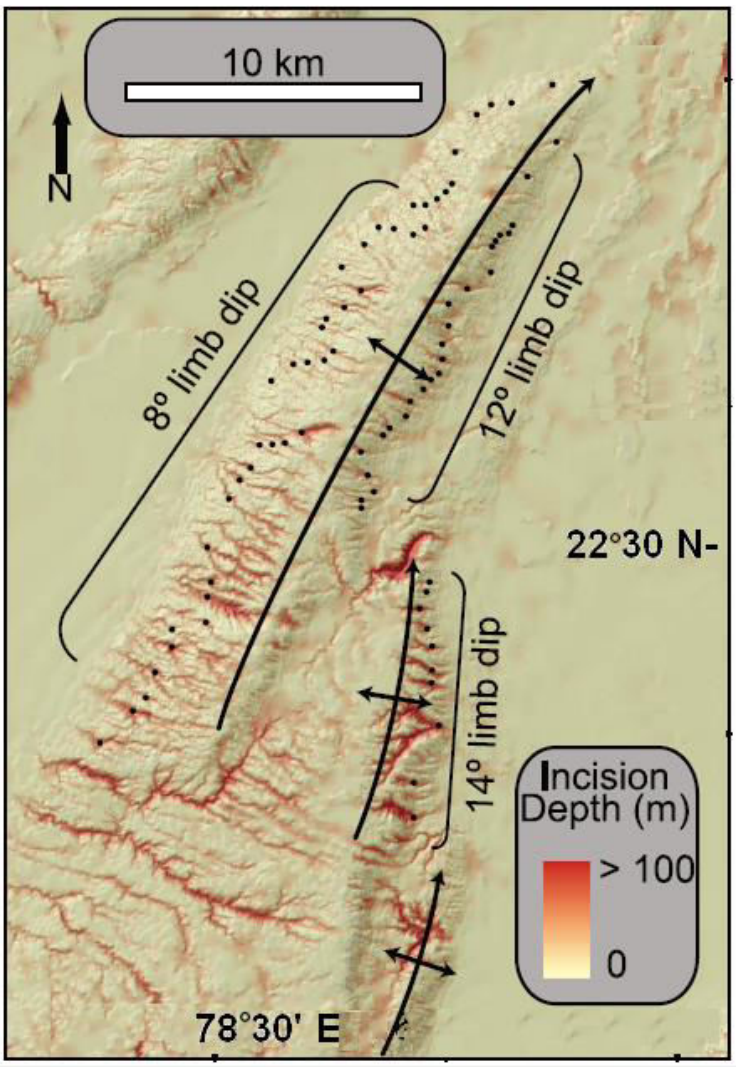

Figure 8. indicates incision depth below the hypothetical pre-erosion surface. Black dots indicate which channels are plotted in Figure 9.

Because these channels are likely antecedent to the growth of the third uplift tip, it is not considered them in this analysis. In contrast, most of the drainages on the northern uplift tips end at the uplift crest, are roughly parallel, and have few tributary junctions. Near the northern tip of each uplift, streams are most deeply incised near the base of the uplift limb. The point of deepest incision moves systematically upstream in channels situated farther south of each uplift tip (Figure 9).

[24] Exposure ages measured through the accumulation of in situ cosmogenic nuclides along the northern tip of South Pachmarhi mountain indicate that this uplift tip has increased by northward propagation during Quaternary times at a rate of 1-2 mm/yr . Deflected antecedent drainages provide additional evidence for the northward propagation of the uplifts. This growth pattern permits the observed spatial pattern of channel incision along the length of the uplift to be recast in terms of channel evolution through time. The argument is that lateral propagation of the South Pachmarhi mountain was episodic rather than constant. Furthermore, if lateral propagation of the uplift had been steady and continuous, the height of the uplift crest would likely increase

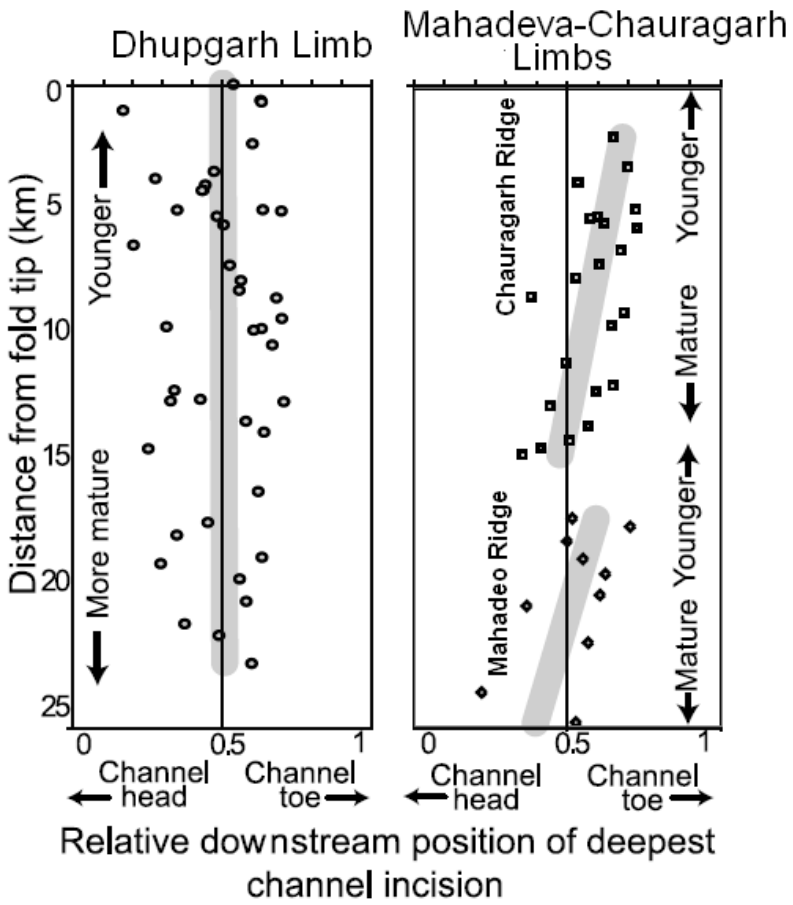

Figure 9. The relative downstream position of deepest incision for all the channels shown in Figure 8. Channels from the west and east limb are shown in the left and right plots, respectively, and are arranged according to the distance of the channel away from the northern tip of Dhupgarh. Channels on the eastern limbs are separated according to the uplift on which they are formed. Gray lines show the best linear fit through each subset of the data.

steadily along strike *[Childs et al.,* 2003; *Manighetti et al.,* 2001]. Instead, elevation profiles across the preerosion surface (Figure 10) indicate that crest height to Mahadeva initially increases south of its northern tip and then remains nearly constant. Thus, it does not be expected that distance from the uplift tip is strictly proportional to the age of initial uplift, only that channels formed at greater distances from the uplift tip are relatively older and more mature than those near the uplift tip.

5.1. Modeling Regional Aggradation and Deformation

[25] Up to this point, the modeling of coupled erosion and deformation has assumed a base level fixed at the toe of the uplift. Nonetheless, the Mahadeva anticline could have formed in an aggradational setting such that the toes of the uplift limbs were steadily covered by sediment. Through time, the structure would still increase above the surrounding plains as long as the rate of tectonic uplift exceeded the rate of aggradation. The three models of planar limb growth through lengthening and rotation show little sensitivity to aggradation at a rate equivalent to half of the relative uplift rate (Figures 11a-11c). This insensitivity is hardly surprising given that both the planar shape of the limbs and underlying kinematics remain unchanged.

[26] The trishear forelimb is characterized by a long, gently sloping toe that steepens near the crest of the uplift. With aggradation at half of the uplift rate, the gentle toe of the trishear forelimb is buried so that only the steeper, updip portion of the uplift is exposed to channel incision (Figure 11e).

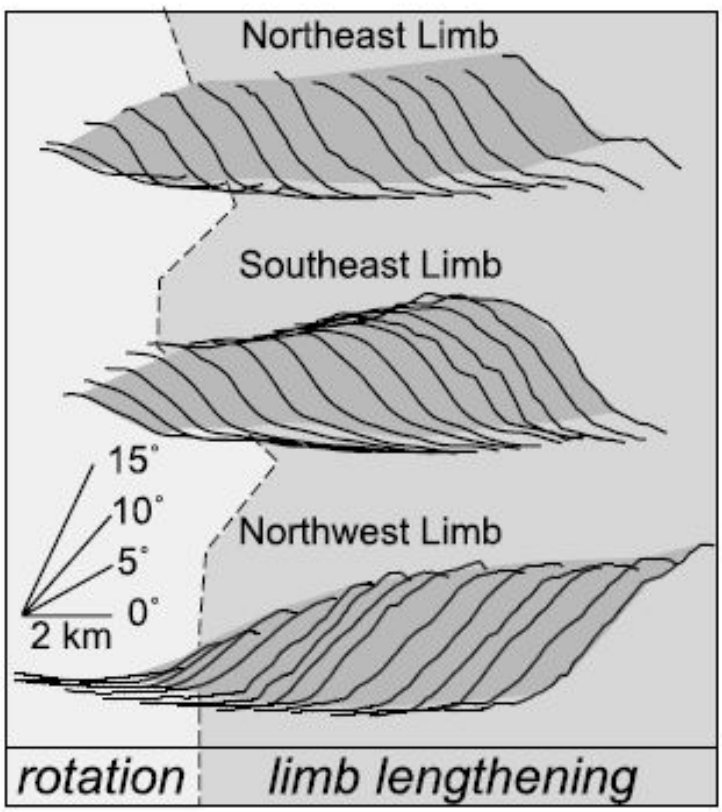

Figure 10. Topographic profiles measured across the pre-erosion surface of Mahadeva uplift limbs. In all cases, limb lengthening is responsible for most uplift growth. The two profiles nearest to the uplift tip on the northeast and northwest limbs indicate some limb rotation in addition to lengthening.

Through time, the exposed portion of the forelimb steepens so that deformation is approximately rotational. Indeed, the channel incision pattern is marked by upstream migration of the point of deepest incision similar to limb rotation models (Figure 11d). This upstream migration stands in sharp contrast to the downlimb migration of the zone of deepest incision that is predicted in the absence of aggradation (Figure 5d).

5.2. Incision Profiles with Different Model Parameters

[27] It is used that the Mahadeva DEM to measure one of the stream power parameters (equation (1)). The value of p describes the increase in drainage area *(A)* with along-stream distance from the divide, where

$$A \propto x^P. \tag{5}$$

[28] On a logarithmic scale, a plot of drainage area against distance from the drainage divide (Figure 12) indicates that the value of 1.1 used in our model accurately describes the rate of drainage accumulation in the upper 1 km of the channels. When data from the entire length of the uplift limbs are considered, 1.3 is a more appropriate value. An increase in *p*enhances erosion of the downstream reaches of modeled channels, because larger p predicts more rapid growth in upstream catchment area and, therefore, in discharge per distance downstream (Figure 13). This more focused erosion at the toe of the uplift leads to more rapid upstream migration of the point of deepest incision (Figures 13b and 13c) in the models of rotation and lengthening through the crest. Similarly, the downstream migration of deepest incision that is observed in the trishear model is enhanced (Figure 12d).

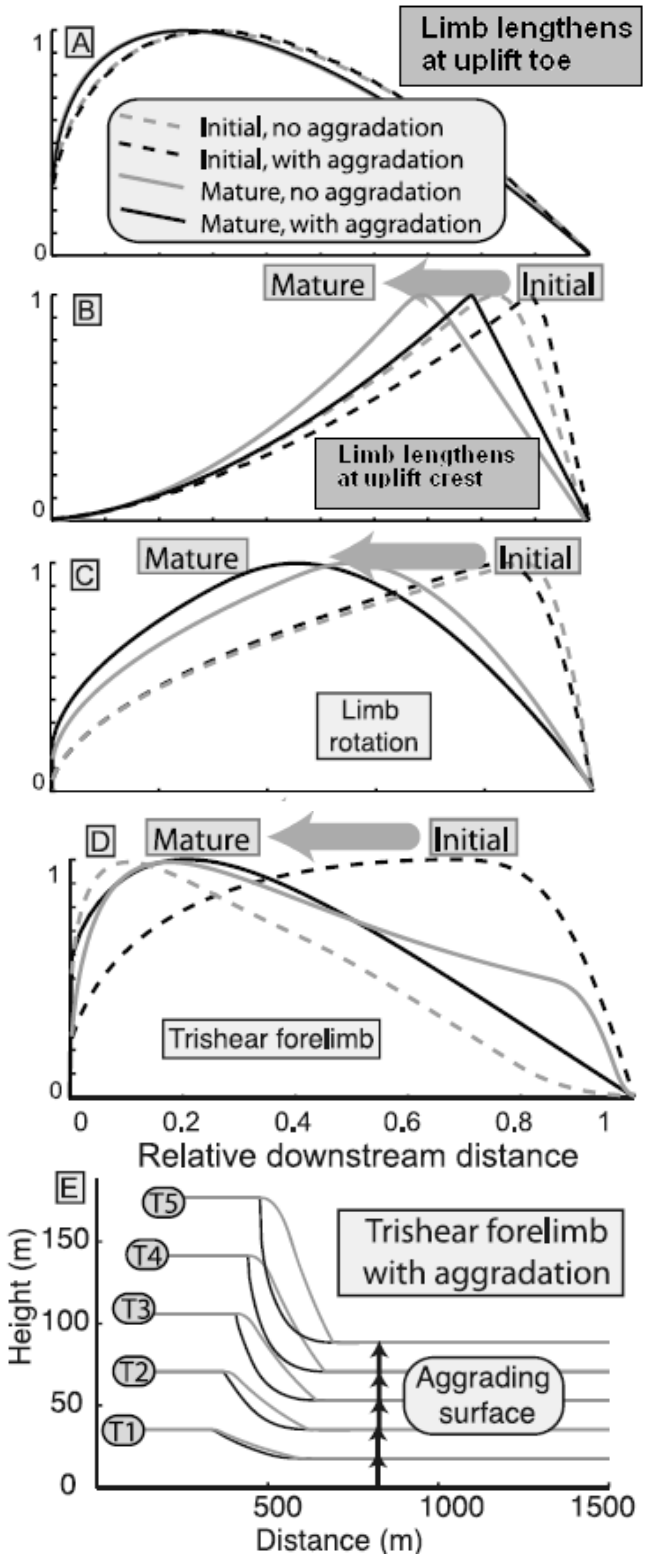

Figure 11. (a-d) Comparisons between original models of planar limb growth (gray curves) and models with aggradation at 50% of the tectonic uplift rate (blackcurves). (e) Surface and channel profiles developed on the trishear forelimb model with 50% aggradation.

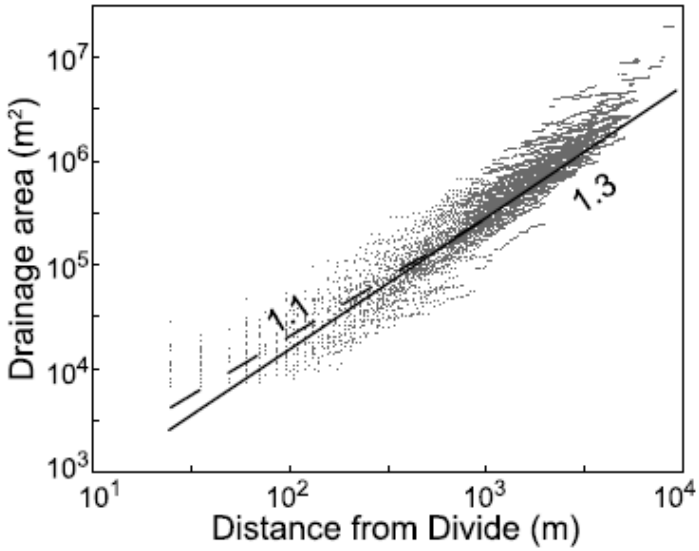

Figure 12. DEM-derived drainage area and streamwise distance from the drainage divide for all the channels in Figure 8. Measurements from the upper 1 km of channels (light gray points) are fit by a power law with exponent of 1.1. Measurements from the entire length of the limbs (dark points) are better fit with an exponent of 1.3.

[29] Increasing *p* without adjusting any other model parameter leads to faster erosion rates and deeper incision. In order to examine the sensitivity of in cisionpro files to changes in *n* (the exponent on both slope and area: order to examine the sensitivity of in cisionpro files to changes in *n* (the exponent on both slope and area: equation (1)), both *n* and the proportionality constant *K* are varied so that the final depth of incision remains near 50 m in all model runs (Figure 14).Because the sensitivity of incision rate to slope is governed by *n* and because limb rotation produces a range of surface slopes without changing drainage area, the limb rotation model is used to explore this aspect of model sensitivity. Although changes in the shape of predicted longitudinal profiles occur as *n* is varied, the upstream migration of deepest incision occurs with little variation in all models.

[30] Longitudinal river profiles developed with different deformation styles, but with identical stream incision parameters (Figure 3e), clearly differ from each other. Nonetheless, the form of longitudinal profiles developed with identical deformation, but with different incision parameters (Figure 14d), is almost as variable as profiles generated with different deformation styles. Despite the dependence of longitudinal profile shape on incision parameters, these parameters are unlikely to differ among channels lying near one another unless underlying bedrock characteristics are changing, too. In general, a change in model parameters that increases incision rates at the toe of the uplift leads to more rapid upstream migration of the point of deepest incision in models of rotation or lengthening through the crest.

6. Discussion

[31] Slip on a buried fault is interpreted to be responsible for the formation of the Mahadeva anticline *[Jackson et al.,* 1996]. Can the observed pattern of channel incision provide additional information on the kinematics of uplift growth?

[32] Substituting the duration of uplift growth for distance from the northern tip of the Mahadeva anticline allows for comparison between our model predictions of channel incision patterns through time (Figures 3, 4, and 5) and the incision patterns observed along the mountain (Figure 9). On the western flank of Mahadeva this ergodic substitution indicates that the point of deepest incision has remained near the channel midpoint throughout uplift evolution (Figure 9). Thus, south of the uplift tip and irrespective of age and position, the channels incising into the west limb of Mahadeva indicate

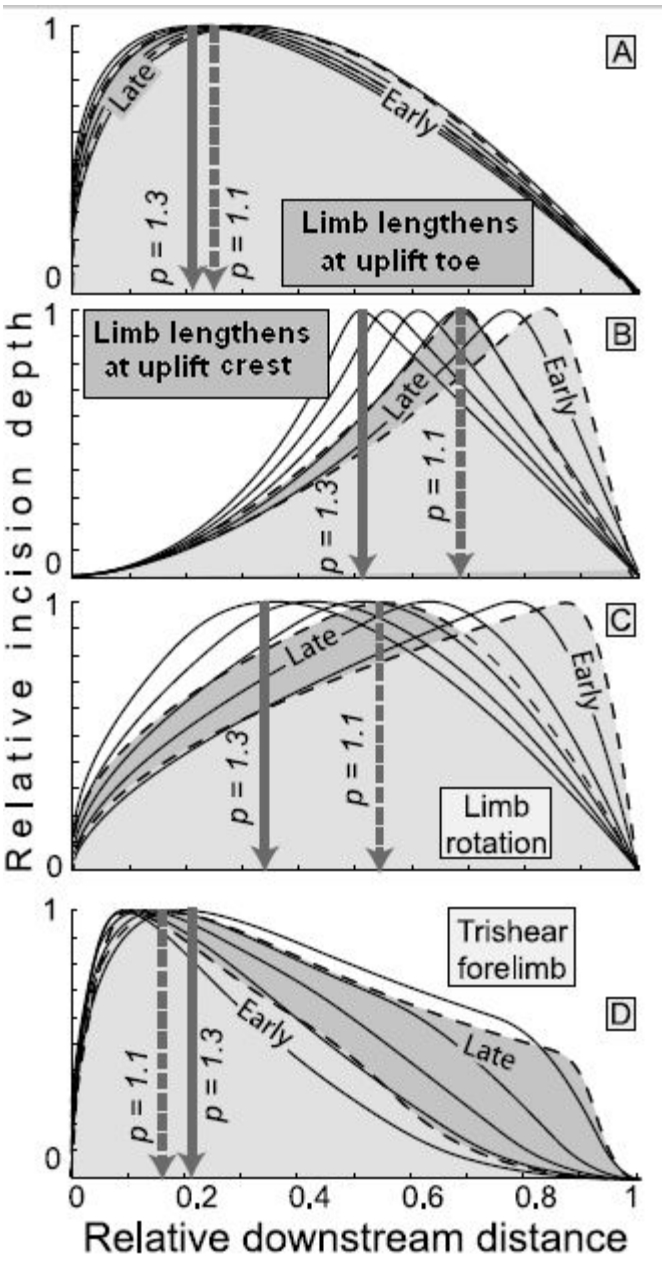

Figure 13. Comparison of relative incision depth between model runs with p =1.1 and p =1.3 (black curves). Dashed curves show early (light gray) and late (dark gray) incision profiles from Figure 5. Increasing the sensitivity of erosion rate to downstream distance by increasing p leads to greater migration of the point of deepest incision (Figures 3b-3d). Dashed arrow highlights the point of deepest incision in original model run. Compare with solid arrow that indicates the analogous point when p = 1.3.

deformation via limb lengthening. This pattern alone cannot, however, conclusively determine the uplift growth history, because the incision pattern predicted for such an actively increasing uplift limb is indistinguishable from the incision

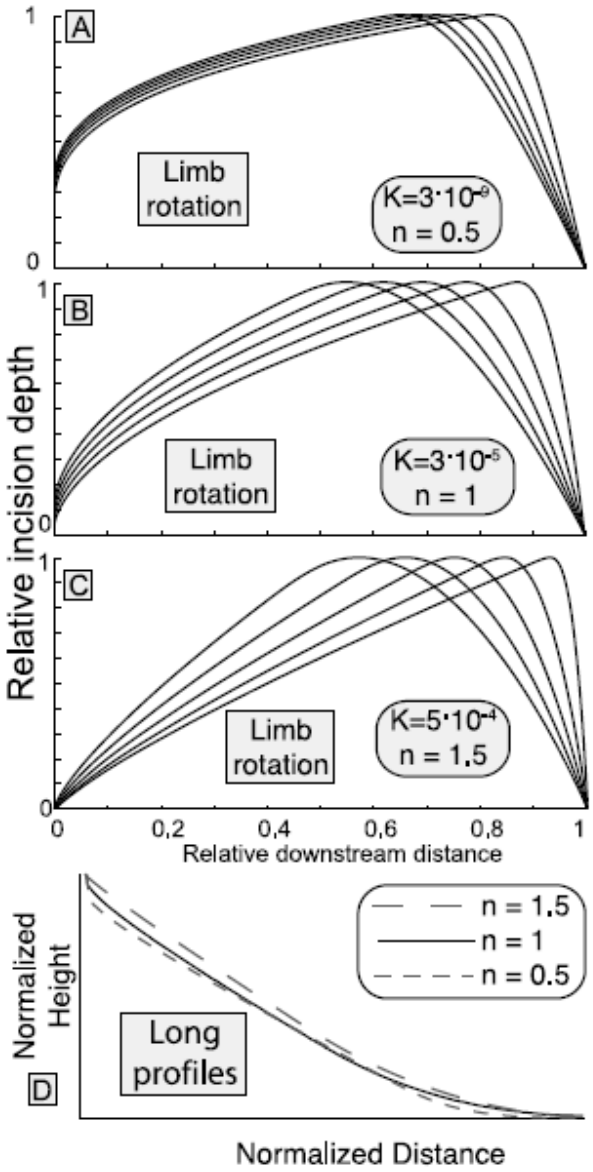

Figure 14. (a-c) Comparison of normalized incision profiles developed during limb rotation with different values of *K* and n. *K* is varied so that the final depth of incision is approximately 50 m in all models. (d) Comparison of longitudinal profiles developed in each model.

[33] The incision patterns on two uplift tips of the eastern flank indicate that initial channel incision is greatest near the uplift toe, but migrates upstream with time as the uplift matures, as shown by the progression of channels from north to south (Figure 9). This observation is consistent with two of the modeled end-member deformation pathways: either limb lengthening through the uplift crest or limb rotation. Elevation profiles across the pre-erosion surface (Figure 10) address this ambiguity. Successive, equally spaced profiles from each of the three uplift limbs are used to represent the evolution of the uplift through time. These profiles indicate that all of the limbs have increased primarily through limb lengthening, although the tip zone along the NE limb shows significant rotational steepening during early stages of growth. Neither topographic profiles nor channel incision patterns alone can constrain Mahadeva's pattern

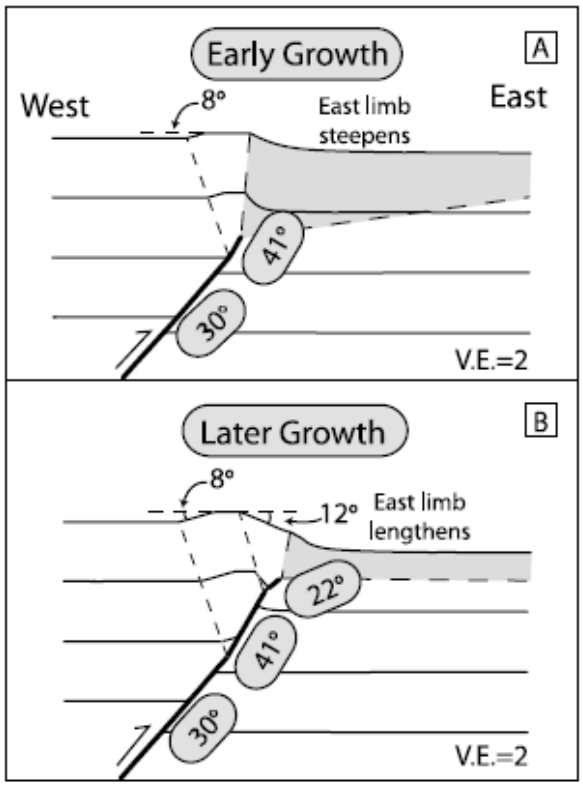

Figure 15. One combination of fault dips and fault propagation patterns that is compatible with the uplift growth history derived from channel incision modeling. The software program 2DMove was used to produce this diagram only

of pattern that would form on a static, previously tilted horizon from which a less resistant cover sequence was progressively stripped away as base level was lowered *[Ramsey et al.,* 2008]. Four observations argue against such a stripping mechanism that would lead to sequential base level lowering. First, the Thickness of Tertiary sediments (a few tens of meters deposited across this region is far smaller than the height of the uplift limb (-500 m). Second, the presence of tors of similar height across the upper flanks and crest of the uplift suggests an equal duration of exposure, as opposed to progressive stripping and exposure. Third, cosmogenic exposure ages along the uplift flanks show no systematic younging toward lower parts of uplift limbs *[Youngson et al.,* 2005], as would be expected if cover rocks were progressively removed. Fourth, if the observed incision patterns are due to this stripping mechanism rather than active deformation, it is expected that the east limb would exhibit the same incision pattern, but it does not. growth. Taken together the two lines of evidence show that the western limb has grown primarily by lengthening through the toe and the eastern limbs have grown primarily by lengthening through the uplift crest with a secondary amount of limb rotation.

[34] In summary, deepest channel incision that remains near the channel midpoint indicates either limb lengthening through the toe or top-down stripping of a cover sequence that causes sequential base level lowering. This ambiguity may be resolved by comparison between opposing uplift limbs, where base level lowering by stripping should produce a symmetrical pattern. Deepest incision near the uplift toe may indicate either limb lengthening through the crest or limb rotation. Examination of topographic profiles across the reconstructed preerosion surface of the uplift (Figure 10) can then be used to determine whether lengthening or rotation dominates. Strongly concave uplift limbs, such as those predicted from trishear models (Figures 1c and 3d), would also be apparent in topographic profiles. Because the surface slope increases near the uplift crest of concave limbs, channel reaches near the uplift crest typically are most deeply incised, despite having relatively small catchment areas.

[35] To be consistent with these findings, a description of the kinematic history of Mahadeva must include lengthening of the west limb throughout uplift growth, early steepening of the east limbs, and later growth of the east limbs by lengthening through the crest. Additionally, drainage asymmetry and patterns of defeated drainages surrounding Mahadeva indicate that Dhupgarh formed first, followed by Mahadeva , and then Chauragarh These geomorphic constraints suggest the following kinematic history. First, Dhupgarh began to form above a blind west dipping reverse fault (Figure 15). During this earliest stage of growth, the west limb would have lengthened through the toe and remained nearly planar. The east limb may have steepened via trishear-style propagation of the fault tip toward the surface (Figure 15a). Given the 8° dip ofthe west limb, this initial period of uplift growth was likely accompanied by at least an 8° increase in the dip of the fault at depth The transition from early steepening of the east limb to lengthening through the toe may be related to a decrease in the dip of the fault as it approached the surface (Figure 15b). Continued slip on this fault would result in lengthening of the west limb through the toe and lengthening of the east limb through the crest. Later growth of the same fault system toward the surface could cause similar steepening and later lengthening of the eastern limb of the younger Mahadeva anticline.

7. Conclusions

[36] Although both growth strata and deformed geomor-phic surfaces can define a history of uplift growth and underpin analyses of uplift kinematics, such data are commonly unavailable. In contrast, almost all emergent uplifts are ornamented with minor channels that have etched their limbs during uplift growth. Here it is shown that the pattern of incision by these channels is sensitive to the kinematics of uplift growth. Uplift growth by limb lengthening through the uplift toe leads to the formation of channels that are most deeply incised near their midpoint: a pattern that shows little change during continued uplift growth. In contrast, either limb lengthening through the crest or limb rotation leads to the formation of channels that are initially most deeply incised near their downstream end. During subsequent uplift growth, this point of deepest incision migrates systematically upstream. Thus, on nascent or propagating uplifts, a spatial pattern in the position of deepest incision on the uplift flanks can be used to deduce the kinematic style of deformation.

[37] Channel incision patterns must be measured relative to a preerosion surface. Constructing such a surface through remnant topography introduces additional uncertainty into measurements of channel incision. Furthermore, descriptions of channel incision that are governed only by drainage area and channel slope may be too simplistic in some regions or at larger spatial scales where changes in sediment load *[Johnson et al.,* 2009; *Sklar and Dietrich,* 1998, 2004; *Yanites and Tucker,* 2010] and precipitation and snowmelt patterns *[Bookhagen and Burbank,* 2010] could dominate.

[38] The incision patterns of nearly 80 channels into the flanks of Mahadeva indicate that channels formed during uplift growth, rather than incising into a static, previously uplifted surface as a cover sequence was stripped away. A combination of channel incision patterns with profiles of uplift topography suggests that the western limb grew by lengthening through the uplift toe, whereas the eastern limb grew primarily via initial rotation followed by lengthening through the uplift crest.

Appendix
A: Numerical Method

[39] The four coupled erosion and deformation models are solved numerically by dividing both the terrace and channel marker lines into 4 m long cells, and calculating erosion and deformation rates at 50 year intervals throughout model development. This computation routine performs the following operations at each time step: (1) calculate the tectonic displacements of each cell of the channel and surface markers according to the model velocity description (equations (2)-(4)); (2) apply the vertical and horizontal displacements to both the channel and surface cells; (3) calculate the slope of the newly displaced channel based on the difference in position between a given cell and the cell immediately downstream; (4) calculate the number of upstream cells that contribute to each channel cell (It does not be

considered that the possible contribution of cells situated beyond the upper limit of the tilted uplift limb.); (5) calculate the erosion rate at each cell (equation (1)) based on the local slope and distance downstream from steps 3 and 4; (6) apply the calculated erosion vertically to the channel cells.

[40] The displaced and eroded channel, as well as the displaced surface, is then used in the next loop of calculations. The horizontal channel reach downstream of the uplift toe defines the local base level. In order to insure that the channel cell situated immediately downstream of the uplift toe does not incise below base level, this calculation scheme does not allow the channel slope upstream of a given cell to contribute to the erosion rate calculation (step 3).

[41] The spatial and temporal resolution of the model allows for efficient computation on a personal computer. In order to test the numerical robustness of this procedure, it is computed that a series of model realizations in which the spatial and temporal step size is decreased by a factor of 2 and 4. Incision depth, the model result of primary interest, changes by <2% and <3% when doubling and quadrupling model resolution.

References

- Ahmadi, R., J. Ouali, E. Mercier, J.-L. Mansy, B. Van-Vliet Lanoe, P. Launeau, F. Rhekhiss, and S. Rafini (2006), The geomorphologic responses to hinge migration in the fault-related folds in the southern Tunisian Atlas, *J. Struct. Geol., 28,* 721-728, doi:10.1016/j.jsg.2006. 01.004.
- Allmendinger, R. W. (1998), Inverse and forward numerical modeling of trishear fault-propagation folds, *Tectonics, 17,* 640-656, doi:10.1029/ 98TC01907.
- Amos, C. B., D. Burbank, D. Nobes, and S. A. L. Read (2007), Geomor-phic constraints on listric thrust faulting: Implications for active deformation in the Mackenzie Basin, South Island, New Zealand, *J. Geophys. Res., 112,* B03S11, doi:10.1029/2006JB004291.
- Bennett, E., J. Youngson, J. Jackson, R. Norris, G. M. Raisbeck, and F. Yiou (2006), Combining geomorphic observations with in situ cos-mogenic isotope measurements to study anticline growth and fault propagation in central Otago, New Zealand, *N. Z. J. Geol. Geophys., 49,* 217-231, doi:10.1080 /00288306.2006.9515161.
- Bookhagen, B., and D. W. Burbank (2010), Toward a complete Himalayan hydrological budget: Spatiotemporal distribution of snowmelt and rainfall and their impact on river discharge, *J. Geophys. Res., 115,* F03019, doi:10.1029/2009JF001426.
- Bullen, M. E. (1999), Late Cenozoic tectonic evolution of the Kyrgyz Range and adjoining Chu Basin: New age constraints from fission-track, (U-Th/He), and magnetostratigraphy, Masters thesis, 110 pp, Penn. State Univ., State College.
- Burbank, D. W., A. Meigs, and N. Brozovic (1996), Interactions of growing folds and coeval depositional systems, *Basin Res.,* 8,199-223, doi:10.1046/j.1365-2117.1996.00181.x.
- Chen, Y.-G., K.-Y. Lai, Y.-H. Lee, J. Suppe, W.-S. Chen, Y.-N. N. Lin,Y. Want, J.-H. Hung, and Y.-T.Kuo(2007),Coseismicfoldscarps and their kinematic behavior in the 1999 Chi-Chi earthquake Taiwan, *J. Geophys. Res., 112,* B03S02, doi:10.1029/2006JB004388.
- Childs, C., A. Nicol, J. J. Walsh, and J. Watterson (2003), The growth andpropagation of synsedimentary faults, *J. Struct. Geol.,* 25,633-648, doi:10.1016/S0191-8141(02)00054-8
- Craw, D., C. Burmountain, and J. Waters (2007), Geological and biological evidence for drainage reorientation during fold of alluvial basins, central Otago, New Zealand, *N. Z. J. Geol. Geophys.*, 50, 367-376,doi:10.1080/00288300709509844.
- Daeron, M., J.-P. Avouac, and J. Charreau (2007), Modeling the shortening history of a fault tip fold using structural and geomorphic records of deformation, *J. Geophys. Res.,* 112,B03S13, doi:10.1029/2006JB004460.
- Erslev, E. A. (1986), Basement balancing of Rocky Mountain foreland folds, *Geology, 14,* 259-262, doi:10.1130/0091-7613(1986)14<259: BBORMF>2.0.CO;2.
- Erslev, E. A. (1991), Trishear fault-propagation folding, *Geology, 19,*617-620, doi:10.1130/0091-7613(1991)019<0617:TFPF>2.3.CO;2.
- Hardy, S., and J. Poblet (2005), A method for relating fault geometry, slip rate and fold data above fault-propagation folds, *Basin Res., 17,* 417-424, doi:10.1111/j.1365-2117.2005.00268.x.

- Howard, A. D., and G. Kerby (1983), Channel changes in badlands, *Geol. Soc. Am. Bull., 94,* 739-752, doi:10.1130/0016-7606(1983)94<739:CCIB>2.0.CO;2.
- Hubert-Ferrari, A., J. Suppe, R. Gonzalez-Mieres, and X. Wang (2007), Mechanisms of active folding of the landscape (southern Tian Shan, China), *J. Geophys. Res., 112,* B03S09, doi:10.1029/2006JB004362.
- Hutton,F. W.,G.H.F.Ulrich,J.G.Black,andJ.McKerrow(1875), *Report on the Geology and Gold Fields of Otago,* 244 pp., Mills Dick,Dunedin, N. Z.
- Jackson, J., R. Norris, and J. Youngson (1996), The structural evolution of active fault and fold systems in central Otago, New Zealand: Evidence revealed by drainage patterns, *J. Struct. Geol., 18*,217-234, doi:10.1016/ S0191-8141(96)80046-0.
- Jackson, J., J.-F. Ritz, L. Siame, G. Raisbeck, F. Yiou, R. Norris, J. Youngson, and E. Bennett (2002), Fault growth and landscape development rates in Otago, New Zealand, using in situ cosmogenic ^{10}Be, *Earth Planet.Sci. Lett., 195,* 185-193, doi:10.1016/S0012-821X(01)00583-0.
- Johnson, J. P. L., K. X. Whipple, L. S. Sklar, and T. C. Hanks (2009),Transport slopes, sediment cover, and bedrock channel incision in the Henry Mountains, Utah, *J. Geophys. Res., 114,* F02014, doi:10.1029/ 2007JF000862.
- Keller, E. A., L. Gurrola, and T. E. Tierney (1999), Geomorphic criteria to determine direction of lateral propagation of reverse faulting and folding, *Geology, 27,* 515-518, doi:10.1130/0091-7613(1999)027 <0515:GCTDDO>2.3.CO;2.
- Kirby, E., and K. Whipple (2001), Quantifying differential rock-fold rates via stream profile analysis, *Geology, 29,* 415-418, doi:10.1130/0091-7613(2001)029<0415:QDRURV>2.0.CO;2.
- Lave, J., and J. P. Avouac (2000), Active folding of fluvial terraces across the Siwalik Hills, Himalaya of central Nepal, *J. Geophys. Res.* , *105,* 5735-5770, doi:10.1029/1999JB900292.
- Manighetti, I., G. C. P. King, Y. Gaudemer, C. Scholz, and C. Doubre (2001), Slip accumulation and lateral propagation of active normal faults in Afar, *J. Geophys. Res., 106,* 13,667-13,696.
- Mueller, K., and J. Suppe (1997), Growth of Wheeler Mountain anticline, California: Geomorphic evidence for fault-bend folding behavior during earthquakes, *J. Struct. Geol., 19,* 383-396, doi:10.1016/S0191-8141(96)00112-5.
- Oskin, M., and D. W. Burbank (2007), Transient landscape evolution of basement-cored folds: Example of the Kyrgyz Range, Tian Shan, *J. Geophys. Res., 112,* F03S03, doi:10.1029/2006JF000563.
- Ramsey, L. A., R. T. Walker, and J. Jackson (2008), Fold evolution and drainage development in the Zagros mountains of Fars province, SE Iran,*Basin Res., 20*,23-48, doi:10.1111/j.1365-2117.2007.00342.x.
- Scharer, K. M., D. W. Burbank, J. Chen, R. J. Weldon, C. Rubin, R. Zhao,and J. Shen (2004), Detachment folding in the southwestern Tian Shan-Tarim foreland, China: Shortening estimates and rates, *J. Struct. Geol.,26,* 2119-2137, doi:10.1016/j.jsg.2004.02.016.